TRAPPED PLASMAS WITH A SINGLE SIGN OF CHARGE

Plasma crystal is not a fanciful oxymoron, but something you can actually make with an easy-to-confine, long-lived nonneutral plasma.

Thomas M. O'Neil

Despite their reputation, not all plasmas are difficult to confine. In fact, one kind of plasma can be kept for long times in a simple apparatus by means of static electric and magnetic fields. It is the kind of plasma that consists exclusively of particles with a single sign of charge. Examples include pure electron plasmas, positive ion plasmas of one or more species, positron plasmas and even electron–antiproton plasmas—all of which have been realized in recent experiments.

These unneutralized collections of charge are called plasmas because they behave in many ways like neutral plasmas, but they are much easier to confine. Indeed, in principle, plasmas with a single sign of charge can be confined forever. In practice, confinement times of days (and even weeks) are routinely achieved, which is one reason why these plasmas provide research opportunities that are not available with neutral plasmas.

A closely related reason is that these unneutralized plasmas can be confined and also be in a state of global thermal equilibrium. This property may sound like it is trivial and shared by all plasmas, but it is not. In fact, neutral plasmas cannot be confined by static electric and magnetic fields and also be in a state of global thermal equilibrium. The incompatibility between confinement and global thermal equilibrium in the case of neutral plasmas is fundamentally the reason why these plasmas are hard to confine. When they are confined, they are not in a state of maximum entropy (or minimum free energy). There is always free energy available to drive instabilities of the sort that have long plagued the confinement of neutral plasmas. By contrast, a confined unneutralized plasma in a state of global thermal equilibrium is guaranteed to be stable and quiescent.

For theory, the possibility of using thermal equilibrium statistical mechanics to describe the late-time plasma state is a large advantage. In effect, Ludwig Boltzmann and Josiah Willard Gibbs solved the complicated many-body physics problem for us. For experiment, a system that is near to thermal equilibrium is more predictable and controllable, and the effect of small controlled deviations from thermal equilibrium can be studied with precision.

Unneutralized plasmas have proven to be excellent subjects for well-controlled studies of a wide range of plasma phenomena over a wide range of parameters. For example, these plasmas can be cooled to the cryogenic temperature range without any recombination, thereby providing experimental access to novel parameter regimes, such as the strong correlation exhibited by Coulomb crystals.

Surprisingly, good confinement persists even if the plasma is created in an initial state that is unstable, and violent fluidlike turbulence ensues. This early-time turbulent evolution can lead to another kind of crystal, in which magnetic-field–aligned vortical structures are annealed by the turbulence to form a regular pattern.

Although there are other fascinating phenomena exhibited by nonneutral plasmas, the focus of this article is on Coulomb and vortex crystals. But we begin with a historical outline of the field, followed by an exploration of the physics of plasma confinement.

THOMAS O'NEIL *is a physics professor at the University of California, San Diego in La Jolla, California.*

Early studies

Dating back nearly half a century, the history of research on trapped clouds of unneutralized charges has roots in both plasma physics and atomic physics.

In 1936, Frans Michel Penning invented the basic confinement configuration for use as a vacuum gauge. A few years later, research on nonneutral plasmas in Penning trap–like field configurations (magnetrons) became part of the effort to produce high-frequency power sources for radar in World War II.

In the late 1960s, nonneutral plasma physics developed rapidly, borrowing techniques and ideas from traditional plasma physics.[1] This development was driven largely by the need to produce new high-frequency power sources and to understand collective effects in intense accelerators and storage rings. The name "nonneutral plasma" was coined in that period.

By the late 1970s, John Malmberg and his collaborators were carrying out experiments on trapped pure electron plasmas at the University of California, San Diego. They made the theoretical proposition that these plasmas with a single sign of charge have exceptionally good confinement properties and might be cooled to a crystal state.[2]

Meanwhile, atomic physicists were also trapping charged particles. In the 1960s, Hans Dehmelt pioneered the use of Penning traps for fundamental studies of individual particles—work for which he received the 1989 Nobel Prize in Physics. Gradually, as the use of Penning traps became widespread in atomic physics and chemistry, some brave investigators began trapping larger and larger numbers of particles. Their experiments left behind the individual particle regime, where atomic physicists had traditionally been comfortable, and moved into the more perilous territory of plasmas and collective effects.

In the 1980s, collaborations began and progress (particularly experimental progress) accelerated. David Wineland and his collaborators at the National Institute of Standards and Technology (NIST) in Boulder, Colorado, who were laser-cooling trapped clouds of ions with the goal of producing accurate atomic clocks, produced small pure ion crystals.[3] Also, antimatter plasmas became available—a development that was stimulated, in part, by efforts to produce antihydrogen at CERN.[4] Indeed, much of the work described here derives from fruitful collaborations between atomic and plasma physicists.

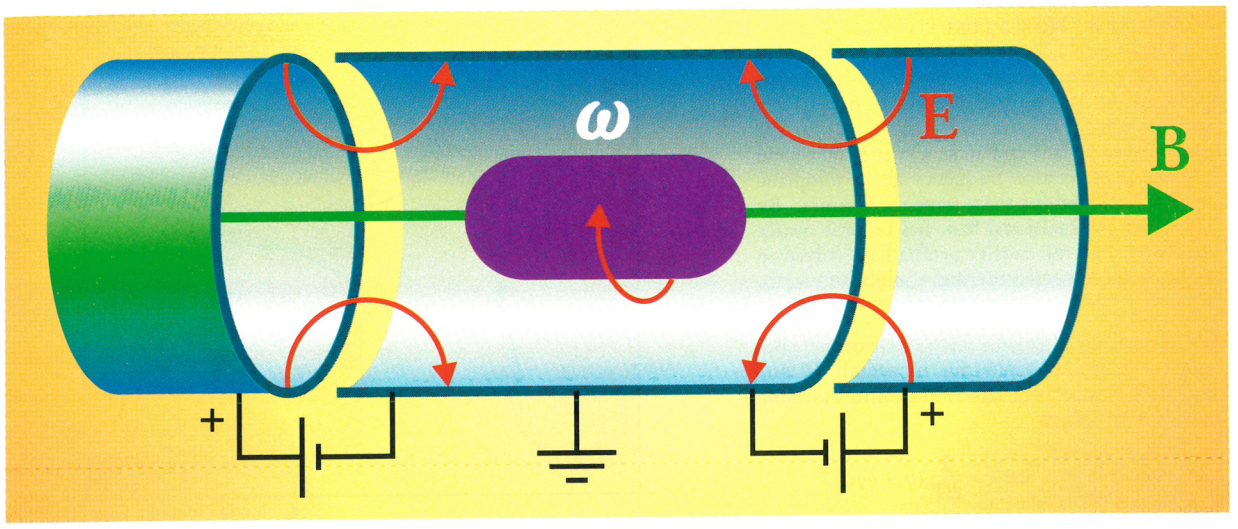

FIGURE 1. A SCHEMATIC DRAWING of a Malmberg–Penning trap. The wall is a conducting cylinder that is divided axially into three sections. The central section is held at ground potential, while the two end sections are held at positive potential (to confine a plasma of positive charges). A uniform axial magnetic field **B** is also present. The plasma (shown in violet) rotates at angular frequency ω in the region of the central grounded section and is confined radially by the magnetic field and axially by the electric fields **E**.

The physics of confinement

Figure 1 shows a schematic drawing of what is now called a Malmberg–Penning trap. Also present is a uniform axial magnetic field $\mathbf{B} = B\hat{\mathbf{z}}$. Here, (r, θ, z) is a cylindrical coordinate system in which the z-axis coincides with the axis of the trap.

Because the plasma is unneutralized, its space charge electrostatic field exerts a large force radially outward. To balance this force and the other radially outward forces (pressure and centrifugal), the plasma rotates about the axis of symmetry of the trap, giving rise to the inwardly directed Lorentz force $(e\mathbf{v}\times\mathbf{B}/c)$, where $\mathbf{v}$ is the rotational velocity. In a sense, therefore, rotation through a magnetic field is like neutralization by a background charge—a useful way to think about these systems, and one that we return to below.

To come to grips with the physics of confinement, we start by considering an ideal trap that is characterized by time-independent trap fields and perfect cylindrical symmetry. Let H be the N-particle Hamiltonian (which is equal in value to the total particle energy) for a system of nonrelativistic, classical charges that interact electrostatically and move in the trap fields. Since it does not depend explicitly on time, H is a constant of the motion. And since H is invariant under rotation, the total canonical angular momentum, P_θ, is also a constant of the motion.

Of course, H and P_θ are not exactly constant for a real plasma in a real trap. Not only do charges slowly radiate energy and angular momentum, but there are also neutrals, which collide with the charges and change their energy and angular momentum. Most important of all, a real trap has small field and construction errors that break the cylindrical symmetry and apply a small torque to the plasma. Nevertheless, by maintaining a good vacuum and by constructing the trap with a high degree of cylindrical symmetry, H and P_θ can remain nearly constant on the timescale required for Coulomb collisions to bring the plasma particles into thermal equilibrium. Thus, we first discuss the confinement and thermal equilibrium states under the assumption that H and P_θ are exact constants, and then discuss the effect of slow changes in these quantities.

To the extent that H (total energy) is conserved, the axial confinement of the particles can be guaranteed simply by placing a high enough potential on the end cylinders. To understand the radial confinement, we invoke the constancy of canonical angular momentum,

$$P_\theta = \sum_j m v_{\theta_j} r_j + \frac{e}{c} A_\theta(r_j) r_j ,$$

where the quantity $mv_{\theta_j}r_j$ is the mechanical part of the angular momentum for the jth particle, and the quantity $(e/c)A_\theta(r_j)r_j$ is the vector potential part. The sum runs over all N particles in the plasma.

For a uniform axial magnetic field, the θ-component of the vector potential is $A_\theta(r) = Br/2$. (Diamagnetic corrections are negligible for the low densities and velocities that we have in mind here.) And for a sufficiently large magnetic field, the vector potential part dominates, and the total angular momentum reduces to the simple form

$$P_\theta \approx \sum_j \frac{eB}{2c} r_j^2 = \frac{eB}{2c} \sum_j r_j^2 .$$

Thus, the constancy of P_θ implies a constraint on the allowed radial positions r_j of the particles—a key concept in the physics of confinement.

Note that this relationship remains valid even if the plasma undergoes complicated turbulent and collisional dynamics, the reason being that the collisions and other internal interactions conserve P_θ.

A simple example illustrates the power of the constraint. Suppose that all the plasma particles initially reside inside a cylindrical region of radius 1 cm—that is, $r_j \le 1$ cm when $t = 0$ for all j—and that the conducting cylindrical wall is located at $r = 10$ cm. To the extent that the sum of $r_j^2(t)$ is conserved, less than 1% of the particles can ever reach the wall at $r = 10$ cm; more than 99% remain confined forever.

By contrast, for a neutral plasma, it is the sum of $e_j r_j^2(t)$ that is constant, which means that an electron and an ion can move to the wall together while preserving the sum. This is precisely what happens in electron–ion collisional transport and in many instabilities.

Thermal equilibrium states

When plasma particles remain confined, they must come

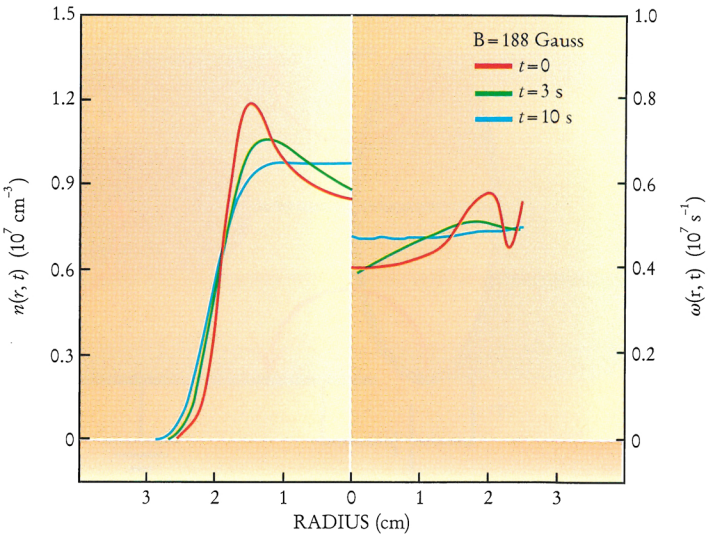

FIGURE 2. HOW A PURE ELECTRON PLASMA settles into a state of thermal equilibrium, as observed experimentally. On the left-hand side, the density $n(r,t)$ is plotted as a function of r for a cut through the plasma mid-plane ($z = 0$) for the three times $t = 0$, 3 and 10 s. On the right-hand side, local rotation frequency at the midplane $\omega(r,t)$ is plotted for these same three times. By $t = 10$ s, the rotational flow has become nearly shearfree, and the density profile has evolved to the expected thermal equilibrium form.

into thermal equilibrium with each other. For a weakly correlated plasma in which H and P_θ are both conserved, the Boltzmann distribution takes the form

$$f = n_0 \left(\frac{m}{2\pi kT}\right)^{3/2} \exp\left[-\frac{1}{kT}(h + \omega p_\theta)\right],$$

where $h = mv^2/2 + e\phi(r,z)$ is the single-particle energy, $p_\theta = mv_\theta r + eBr^2/2c$ is the single-particle canonical angular momentum and $\phi(r, z)$ is the mean-field electric potential.[1,2]

The combination

$$h + \omega p_\theta = \frac{m}{2}\left[v_z^2 + v_r^2 + (v_\theta + \omega r)^2\right]$$

$$+ e\phi(r,z) - \frac{m\omega^2}{2} r^2 + \frac{eB\omega}{2c} r^2$$

is the single-particle energy as viewed in a frame that rotates with frequency $-\omega$. (Positively charged plasmas rotate in a negative sense relative to $B\hat{z}$.)

The velocity distribution is Maxwellian in the rotating frame, so, from a fluid perspective, the flow is shearfree (rigid rotor flow). If the flow were not shearfree, viscous forces would produce entropy, which is impossible in a state of maximum entropy.

The density distribution is determined by three potentials—namely, the electric potential $\phi(r, z)$, the centrifugal potential $-m\omega^2 r^2/2$, and the potential $eB\omega r^2/2c$. This last potential is associated with the electric field induced by rotation through the magnetic field. It is this potential that provides the radial confinement.

To see that the distribution, in fact, does correspond to a confined plasma, note that $\phi(r, z)$ forces the distribution to be exponentially small at each end (assuming that the potential on the end electrodes is turned up sufficiently high) and that the potential $eB\omega r^2/2c$ forces the distribution to be exponentially small at large r (assuming that B is sufficiently large). Of course, the conducting wall is assumed to be outside the radius where the distribution becomes exponentially small. Note, too, that such thermal equilibrium distributions do not correspond to confinement for a neutral plasma. The sign of the charge enters $e\phi(r,z)$ and $eB\omega r^2/2c$, so confinement of electrons means nonconfinement of ions.

The density normalization n_0, temperature T and rotation frequency ω are determined by the three quantities N, H and P_θ. Because effects such as radiation, collisions with neutrals and interaction with small field errors produce a slow evolution in the values of H and P_θ, the values of n_0, T and ω will slowly change with time.

If no countermeasures are taken to oppose the ambient torque and heating (or cooling), n_0, T and ω will evolve in such a way that the plasma will escape.

However, counteracting torques and heating (or cooling) can be applied using laser beams (or rotating field asymmetries) to keep H and P_θ constant.[5] In this way, the plasma can be maintained in steady state for weeks at a time, or be put into some new thermal equilibrium state that is more convenient for a particular experiment.

The electric potential $\phi(r, z)$ is determined largely by the plasma charge density itself, so Poisson's equation must be solved with the charge density given by the thermal equilibrium density distribution. Fortunately, the self-consistent solutions for potential and density have a simple universal character.[1,2] The density is nearly constant out to some surface of revolution, where it drops to zero in a few Debye screening lengths. That length is given by $\lambda_D = (k_B T/4\pi ne^2)^{1/2}$, where n is the density (by definition, plasma is a collection of charges that is large compared to the Debye length).

This general picture of the plasma is easy to understand physically. In the thermal distribution, the two potential energy terms due to rotation are both quadratic in r. Suppose that the radial confinement is provided not by rotation through a magnetic field, but by the electrostatic field from an imaginary cylinder of uniform negative charge. The potential energy of a positive charge e in such a field would also be quadratic in r, so the two terms due to rotation can be interpreted as such a potential energy. The electric potential for a cylinder of uniform charge density $-en_-$ is $\phi_- = \pi en_- r^2$, so the required choice

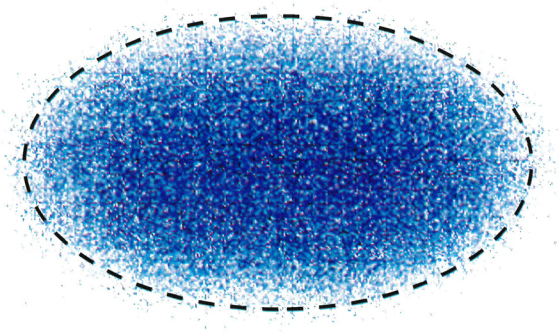

FIGURE 3. SIDE VIEW OF A PLASMA that consists of 8×10^4 beryllium ions in a quadratic trap potential, together with the best-fitting elliptical envelope.

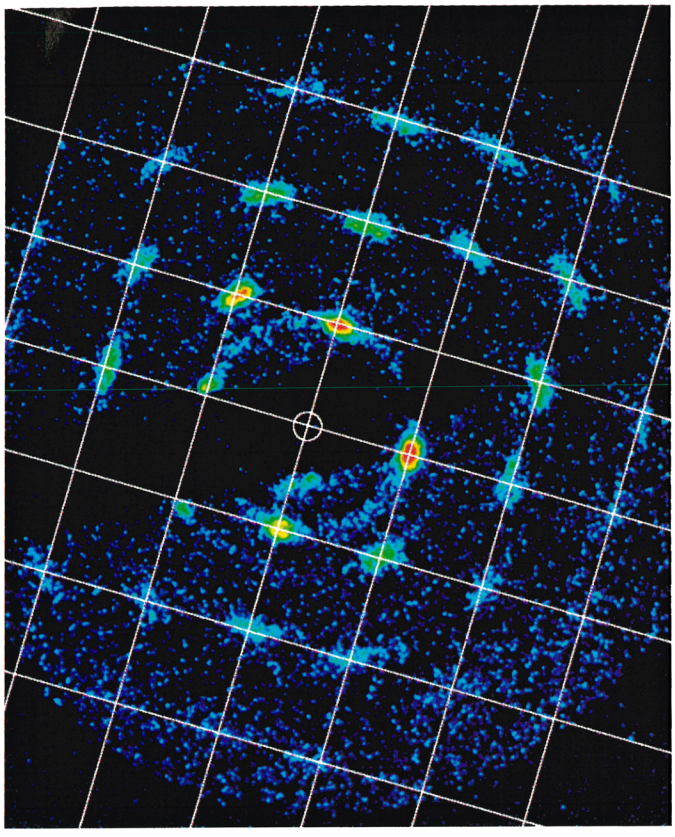

FIGURE 4. TIME-RESOLVED BRAGG DIFFRACTION PATTERN obtained by scattering laser light from a trapped plasma of $N = 8 \times 10^4$ Be^+ ions. The effect of plasma rotation was removed by stroboscopically imaging the scattered light. A body-centered cubic lattice aligned along the <100> axis would generate a spot at each intersection of the grid lines overlaid on the image.

for the density is $-m\omega^2/2 + eB\omega/2c$. For this choice, the thermal equilibrium distributions for the two systems differ only by a velocity shift due to rotation—that is, $v_\theta \rightarrow v_\theta + \omega r$. Otherwise, the density distributions are identical.

This equivalence is useful because we know what will happen if we put a collection of positive charges into a potential well produced by a cylinder of uniform neutralizing charge (and by the positively biased end cylinders). The positive charges will go to the bottom of the well, matching their density to that of the negative charge—that is, $n(r, z) = n_-$. And they will fill the well out to some surface of revolution where the supply of charges is exhausted and where the density will drop to zero.

Figure 2, from the UCSD neutral plasma group, shows how a pure electron plasma settles into a state of thermal equilibrium through collisional transport.[6] A signature of thermal equilibrium is shear-free rotational flow, but, for an arbitrary initial equilibrium, the rotation frequency is not uniform in r. The shears in the rotational flow give rise to viscous forces (due, microscopically, to collisions) that drive the plasma into a state of rigid rotation. We can see in figure 2 that, by $t = 10$ s, the density profile has evolved to the expected thermal equilibrium form, and that the rotation frequency has become nearly uniform.

Detailed studies of collisionally driven transport across magnetic fields led the UCSD group to the discovery of a new transport theory.[7] Nonneutral plasmas typically exist in a parameter regime where the cyclotron radius for a particle is small compared to the Debye length. In this regime, the new theory predicts particle and heat fluxes that are much larger than those predicted by traditional theory, but that are in good agreement with measurement.

For an important class of experiments, the surface of revolution at which the plasma density drops to zero is a spheroid (an ellipse of revolution).[8] Except at the thin surface sheath, the plasma density is uniform within the spheroid. In these experiments, which atomic physicists favor, the plasma cloud is small compared to the size of the trap, and the Taylor expansion of the trap potential is nearly quadratic over the region of the cloud. It is not too surprising, therefore, that the quadratic trap potential gives rise to a quadratic surface of revolution like an spheroid.

Figure 3, from the NIST ion storage group, shows a side-view image of a plasma that consists of about 8×10^4 beryllium ions in a quadratic trap potential, together with the best-fitting elliptical surface envelope. The aspect ratio of the fitted ellipse (length ÷ diameter = 1.763) is in good agreement with the aspect ratio 1.75 predicted by theory for the measured rotation frequency and known trap parameters.

By using laser beams to manipulate the values of H and P_θ, the experimenters were able to lead the plasma through the full range of thermal equilibrium states (consistent with the constraint of small Debye length). The measured plasma shape was in quantitative agreement with theory over the full range.[5]

Theoretical analysis yields accurate, analytic descriptions of not only the equilibrium shape of these small spheroidal plasmas, but also the linear modes of oscillation about the equilibrium state (including all plasma modes, upper hybrid modes and cyclotron modes).[9] The theory for the modes, like that for the equilibrium shape, assumes that the Debye length is small. For the low-order modes checked so far, both the predicted frequencies and the spatial structure of the eigenmodes are in excellent agreement with measurement and simulation. These small spheroidal plasmas are possibly the best understood and best controlled plasmas currently in existence.

Coulomb crystals

Small spheroidal plasmas have been laser cooled to temperatures in the range of a few millikelvins. As the temperature is reduced, the random kinetic energy of a particle becomes smaller than the Coulomb interaction energy between neighboring particles, and interparticle correlation becomes important. First, the system of particles enters a state with the short-range order characteristic of a fluid; then it suffers a phase transition to a state with long-range order—that is, to a crystal state.

A measure of the correlation strength is the coupling parameter $\Gamma = e^2/ak_BT$, where the Wigner–Seitz radius a, which is defined as $(3/4\pi n)^{1/3}$, is essentially the interparticle spacing, and where Γ is the ratio of the Coulomb interaction energy between neighboring particles e^2/a to the random thermal energy for a particle k_BT, so the Coulomb interactions can establish strong correlations when $\Gamma \gg 1$.

To develop a theory for the crystal structure, we return to the equivalence between the thermal distribution for a magnetically confined plasma and a plasma that is confined by a cylinder of uniform neutralizing charge. Previously, we established this equivalence for the Boltzmann

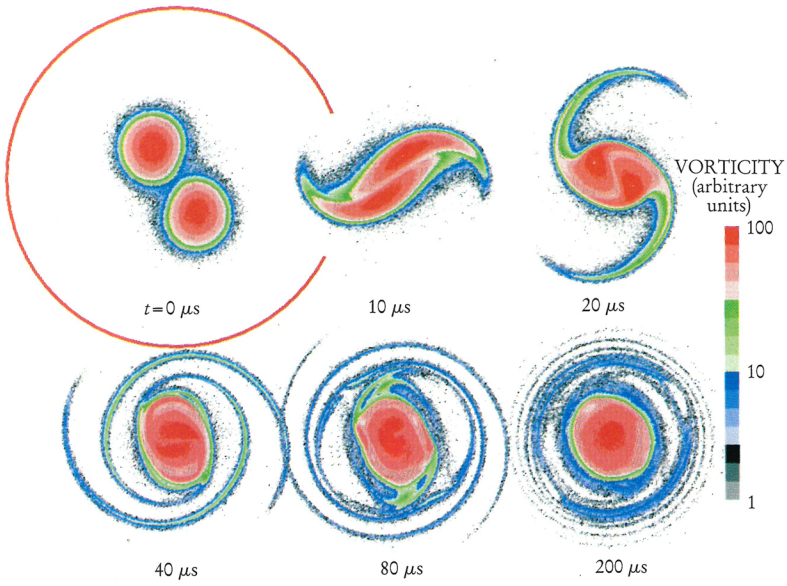

FIGURE 5. A SEQUENCE OF EXPERIMENTAL images that illustrate vortex merger, with intensity of vorticity (z-integrated electron density) indicated by color. The large red circle in the first image indicates the location of the wall.

distribution, but the argument is easily extended to the Gibbs distribution.[2]

As an N-particle distribution, the Gibbs distribution includes all information about spatial correlations, so we may conclude that the microscopic order is the same for the two systems. A system of point charges in a uniform neutralizing background charge is called a one component plasma (OCP) and has been a favorite theoretical model for the study of correlation effects. For a plasma large enough that bulk properties predominate, we can simply adopt the well-known results for a homogeneous OCP and apply them to the magnetically confined plasma. For example, it has been known for many years that the lowest energy state of such a plasma is a body-centered cubic (BCC) crystal. The lattice spacing is set by the density, which again is equal to that of the imaginary neutralizing charge—that is, $n = n_- = B\omega/2c\pi e - m\omega^2/2\pi e^2$.

Figure 4 shows a time-resolved Bragg diffraction pattern, which Wayne Itano (NIST, Boulder) and his collaborators obtained by scattering laser light from a spheroidal plasma of 8×10^4 Be^+ ions.[10] The pattern from a crystal that rotates about the laser beam would appear as nested rings, but here the effect of the rotation was removed by stroboscopically imaging the scattered light (with a CCD camera). The diffraction peaks all lay on the intersections of a square grid, which is consistent with a single BCC crystal oriented so that the incident laser beam is along the crystal's <100> axis. An angular calibration was made, and the agreement between the observed and calculated grid spacing was within the uncertainty of the measurement (about 1%). Other crystal structures (for example, face-centered cubic) were occasionally observed, but the BCC structure predominated for sufficiently large plasmas.

In earlier experiments with smaller plasmas, the ions were observed to lie on nested surfaces of revolution.[3] Numerical studies by various groups showed that this shell structure is the thermal equilibrium state for smaller plasmas in which surface effects predominate.[11] One can think of a given shell as a lattice plane that has been deformed to follow the spheroidal surface of the plasma.

In related experiments conducted by Herbert Walther and his collaborators (Max Planck Institute for Quantum Electronics, Garching, Germany), even smaller numbers of charges were confined and laser cooled in Paul (radio frequency) traps, and Coulomb clusters with a rich variety of structures were observed.[12] The structures and phase transitions between the structures were understood by calculating the minimum energy states.[13]

Vortex dynamics and turbulence

Trapped nonneutral plasmas, like neutral plasmas, exhibit a rich variety of collective dynamics. Here, we focus on a particularly simple form of collective dynamics that has been studied with long columns of pure electron plasma.

When a typical electron's cyclotron and axial bounce frequencies are high, the associated oscillations are averaged over in low-frequency motions. (Axial bouncing is the movement of electrons back and forth in the trap parallel to the magnetic field.) In this case, we can think of the plasma as consisting of long rods (bounce-averaged electrons) that move across the magnetic field with the $\mathbf{E} \times \mathbf{B}$ drift velocity, $\mathbf{v}_d = c\,\nabla\phi \times \hat{\mathbf{z}}/B$. The density $n(r,\theta,t)$ evolves under this flow field according to the continuity equation, and the bounce-averaged potential $\phi = \phi(r,\theta,t)$ is determined, in turn, by the density through Poisson's equation.

An interesting feature of these two-dimensional drift Poisson equations is that they are identical to the equations for the two-dimensional flow of an ideal—that is, incompressible and inviscid—fluid. The electric potential corresponds to the stream function and the density to the vorticity. Thus, the plasma can be used to model the two-dimensional flow of an ideal fluid. Surprisingly, experiments with a pure electron plasma offer advantages over experiments with a tank of water!

For example, the vorticity (electron density) can be measured directly by dumping the plasma out along the magnetic field lines to a phosphorus screen that is imaged by a CCD camera. This operation is accomplished simply by switching the confinement voltage on the appropriate end cylinder to ground potential. Another advantage is that the plasma is well separated from the ends and walls during the two-dimensional flow, so there are no boundary layers at the ends and edge to complicate the flow. Moreover, the effective viscosity of the plasma is very low.

Figure 5, from the UCSD nonneutral plasma group, shows a sequence of experimental images that illustrate vortex merger, with vorticity (z-integrated electron density) indicated by color. The image labeled $t = 0$ μs was obtained by dumping the plasma almost immediately after two adjacent vortices (electron columns) were created. This image encapsulates the initial conditions for the evolution. The large red circle indicates the location of the wall.

The other images were obtained by starting from the same initial condition, but then allowing the two-dimensional evolution to proceed for 10, 20, 40, 80 and 200 μs before executing the dump. The measurement destroys the plasma, so each image was obtained with a different plasma. However, the shot-to-shot reproducibility was sufficiently good that a movie of the merger process could be made.

The time to merge was studied as a function of the

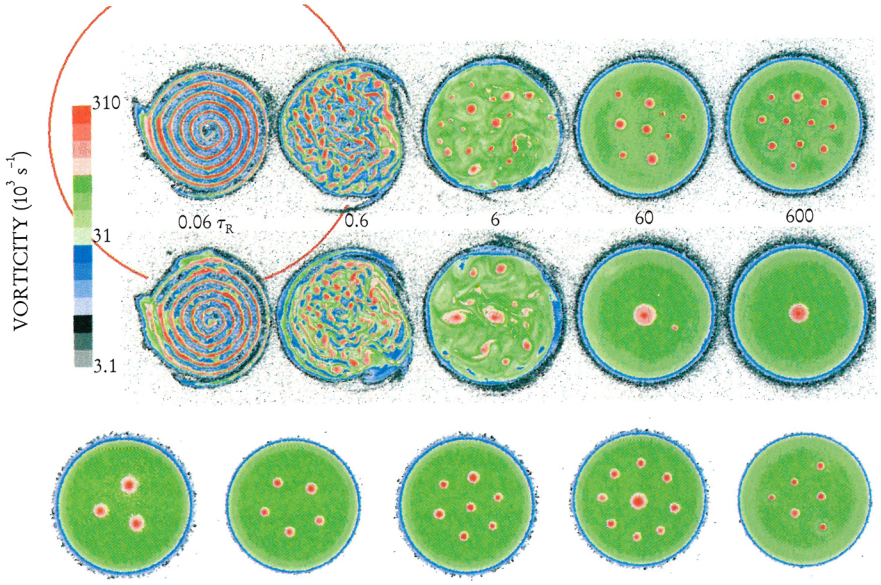

FIGURE 6. EXPERIMENTAL IMAGES of the vorticity distribution are shown for two turbulent evolutions (two top rows). In the second row of images, vortex merger processes led to a single large vortex at the center of a patch of lower intensity background vorticity, similar to the last panel of figure 5. In the top row, cooling of the vortex system through interaction with the background vortex patch annealed the vortices into a local energy minimum (vortex crystal), thereby arresting further evolution and merger. The bottom row of images is a selection of observed vortex crystals.

ratio S/D, where S is the separation between the centers and D is the diameter of the two nearly identical vortices.[15] For values of S/D up to about 1.5, the time to merge was about the time taken by the two vortices to orbit one another (the case for figure 5), but as S/D was increased through the narrow interval from 1.5 to 1.7, the time to merge increased by nearly five orders of magnitude. Above this transition, merger was delayed until viscous effects broadened the vortices. The timescale separation of five orders of magnitude illustrates the advantages of using the plasma to model the flow of ideal fluids.

In similar experiments, Joel Fajans and his Berkeley collaborators have studied the stability of a single vortex against distortion.[15] In the language of fluid dynamics, the distortion away from circular cross section is produced by subjecting the vortex to external shear flows. In the plasma experiment, these flows are produced by applying different voltages to azimuthally separated sectors of the cylindrical wall.

Recently, the UCSD group observed a surprising and novel state called a vortex crystal.[16] Two turbulent evolutions are illustrated by the vorticity images in the two top rows of figure 6. Highly filamented vorticity distributions (spirally wound sheets of electrons) were produced by trapping electrons from a spiral electron source. The spiral vorticity structure can be seen in the initial images, which were obtained by dumping the plasma shortly after trapping, when $t = 0.06\ \tau_R$ (τ_R is the rotation period of the column). By the time of the second images ($t = 0.6\ \tau_R$), local Kelvin–Helmholtz instabilities had produced an irregular field of many small and intense vortices (red regions). The subsequent chaotic advection caused many vortices to merge, so that, by the time of the third images ($t = 6\ \tau_R$), there were fewer but larger vortices. Furthermore, parts of vortices were sheared into long filamentary tails, the remnants of which formed a patch of low-intensity background vorticity (the green region in figure 6).

The presence of the background vorticity is important, because the system of vortices was effectively cooled by stirring the background vorticity. Indeed, there was a competition between the cooling and the tendency of the vortices to merge.

In the second row of images, the merger processes went to completion and left a single large vortex at the center of the background vortex patch. In the top row of images, cooling annealed the vortex system into a local energy minimum (vortex crystal) that arrested further mergers.

Once formed, the vortex crystals survived as rigidly rotating patterns until viscous effects became important when t was about $10^4\tau_R$. Although the initial images for the two evolutions look similar, they are, in fact, slightly different as a result of different settings used for the electron source. The settings for the top row of images systematically produced a vortex crystal, but the number of vortices in the crystal varied from shot to shot. The bottom row of images in figure 6 is a selection of some of the vortex crystals that have been observed.

Similar vortex crystals have been observed in rotating superfluids, where the energy loss from the vortex system occurs through friction on the normal fluid.[17] Of course, the vortex crystals are two-dimensional cousins of the three-dimensional crystals discussed earlier, since the vortices can be thought of as charged rods that interact through a logarithmic potential, rather than the usual Coulomb potential for point charges.

The free decay of two-dimensional turbulence has engaged the interest of many theorists, and the unexpected discovery of vortex crystals in the final state shows that the problem is richer than originally thought.

Vortex crystals prompt many questions. For instance: What sets the number and size of the surviving vortices? What is the cooling mechanism—that is, the mechanism by which energy is transferred from the intense vortices to the background vorticity? Can vortex crystals appear in the final state of a flow in which both signs of vorticity are present?

At first glance, the organization of the intense vortices into a regular array that starts from a random-looking turbulent state may seem to contradict the second law of thermodynamics. However, one must remember that the entropy of the background vorticity is increasing.

A recent theory put forward by De-Zhe Jin and Dubin maximizes the entropy of the system, which consists of background vorticity plus a specified set of intense vortices.[18] The number and profile of the intense vortices are specified, and the entropy is maximized subject to constraints that include the incompressible nature of the flow. The theory successfully predicts the final shape of the background vorticity profile and the locations of the intense vortices.

A broader perspective

The above discussion focuses on two opposite limits of research with trapped nonneutral plasmas: the late-time thermal equilibrium states and the early-time turbulence. These two topics were chosen to illustrate the range of such research, but many other interesting topics could have been discussed—the linear modes of oscillation for the trapped plasmas, the novel nature of the collisional relaxation to thermal equilibrium, centrifugal separation of multispecies plasmas, the late-time dynamical control of the plasma temperature and rotation frequency, use of the plasmas in high-precision atomic clocks and efforts to produce antihydrogen.

The range of physics that is being explored with these simple plasma systems is surprisingly broad and touches on issues of interest to plasma physics, atomic physics, condensed matter physics and fluid dynamics. And a growing number of researchers are using these remarkable plasmas for a widening variety of purposes.

The author thanks John Bollinger, Fred Driscoll, Daniel Dubin, Kevin Fine and Cliff Surko for help and guidance in the preparation of this article. Research on these nonneutral plasma systems has been supported largely by the National Science Foundation, the Office of Naval Research and the National Institute of Standards and Technology.

References

1. R. C. Davidson, *Theory of Nonneutral Plasmas*, Benjamin, Reading, Mass., (1974). R. C. Davidson, *Physics of Nonneutral Plasmas*, Addison-Wesley, Redwood City, Calif. (1990).
2. J. H. Malmberg, T. M. O'Neil, Phys. Rev. Lett. **39**, 1333 (1977). D. H. E. Dubin, T. M. O'Neil, Rev. Mod. Phys. **71** (1) 20 (1999).
3. S. L. Gilbert, J. J. Bollinger, D. J. Wineland, Phys. Rev. Lett. **60**, 2022 (1988).
4. R. G. Greaves, C. M. Surko, Phys. Plasmas **4**, 1528 (1997). G. Gabrielse *et al.*, Phys. Rev. Lett. **57**, 2504 (1986). M. H. Holzscheiter *et al.*, Phys. Lett. A **214**, 279 (1996).
5. T. M. O'Neil, D. H. E. Dubin, Phys. Plasmas **5**, 2163 (1998). J. J. Bollinger, D. J. Wineland, D. H. E. Dubin, Phys. Plasmas **1**, 1403 (1994). X. P. Huang, F. Anderegg, E. M. Hollmann, T. M. O'Neil, C. F. Driscoll, Phys. Rev. Lett. **78**, 875 (1997). X. P. Huang, J. J. Bollinger, T. B. Mitchell, W. M. Itano, Phys. Rev. Lett. **80**, 73 (1998).
6. C. F. Driscoll, J. H. Malmberg, K. S. Fine, Phys. Rev. Lett. **60**, 1290 (1988).
7. D. H. Dubin, Phys. Plasmas **5**, 1688 (1997).
8. L. R. Brewer, J. D. Prestage, J. J. Bollinger, W. M. Itano, D. J. Larson, D. J. Wineland, Phys. Rev. A **38**, 859 (1988).
9. D. H. E. Dubin, Phys. Rev. Lett. **66**, 2076 (1991). T. B. Mitchell, J. J. Bollinger, X. P. Huang, W. M. Itano, Optics Express **2**, 316 (1998). G. W. Mason, R. L. Spencer, J. A. Bennett, Phys. Plasmas **3**, 1502 (1996).
10. W. M. Itano, J. J. Bollinger, J. N. Tan, B. Jelenkovic, X.-P. Huang, D. J. Wineland, Science **279**, 686 (1998).
11. A. Rahman, J. P. Schiffer, Phys. Rev. Lett. **57**, 1133 (1986). H. Totsuji, in *Strongly Coupled Plasma Physics*, F. J. Rogers, H. W. DeWitt, eds., Plenum, New York, (1987), p. 19. D. H. E. Dubin, T. M. O'Neil, Phys. Rev. Lett. **60**, 511 (1988).
12. H. Walther, Physica Scripta Topical Issues **59**, 360 (1995). G. Birkl, S. Kassner, H. Walther, Nature **357**, 310 (1992).
13. R. W. Hasse, J. P. Schiffer, Ann. Phys. (NY) **203**, 419 (1990). H. Totsuji, J. L. Barrat, Phys. Rev. Lett. **60**, 2484 (1988).
14. K. S. Fine, C. F. Driscoll, J. H. Malmberg, T. B. Mitchell, Phys. Rev. Lett. **67**, 588 (1991).
15. J. Notte, A. J. Peurrung, J. Fajans, R. Chu, J. S. Wurtele, Phys. Rev. Lett **69**, 3056 (1992). J. Fajans, E. Yu., J. E. McCarthy, Phys. Plasmas **6**, 12 (1999). E. Yu, Backhaus, J. Fajans, J. S. Wurtele, Phys. Plasmas **6**, 19 (1999).
16. K. S. Fine, W. G. Flynn, A. C. Cass, C. F. Driscoll, Phys. Rev. Lett. **75**, 3277 (1995).
17. E. J. Yarmchuk *et al.*, Phys. Rev. Lett. **43**, 214 (1979). L. J. Campbell, R. M. Ziff, Phys. Rev. B **20**, 1886 (1979).
18. D. Z. Jin, D. H. E. Dubin, Phys. Rev. Lett. **80**, 4434 (1998). ■